Applied Physics Letters

Design and demonstration of efficient transparent 30% Al-content AlGaN interband tunnel junctions

Cite as: Appl. Phys. Lett. **122**, 081108 (2023); https://doi.org/10.1063/5.0122919
Submitted: 26 August 2022 • Accepted: 09 February 2023 • Published Online: 23 February 2023

Agnes Maneesha Dominic Merwin Xavier, Arnob Ghosh, Sheikh Ifatur Rahman, et al.

AIP Publishing

Applied Physics Letters ARTICLE scitation.org/journal/apl

Design and demonstration of efficient transparent 30% Al-content AlGaN interband tunnel junctions

Cite as: Appl. Phys. Lett. **122**, 081108 (2023); doi: 10.1063/5.0122919
Submitted: 26 August 2022 · Accepted: 9 February 2023 ·
Published Online: 23 February 2023

View Online Export Citation CrossMark

Agnes Maneesha Dominic Merwin Xavier,[1,a)] Arnob Ghosh,[1] Sheikh Ifatur Rahman,[1] Andrew Allerman,[3] Shamsul Arafin,[1] and Siddharth Rajan[1,2]

AFFILIATIONS

[1]Department of Electrical and Computer Engineering, The Ohio State University, Columbus, Ohio 43210, USA
[2]Department of Materials Science and Engineering, The Ohio State University, Columbus, Ohio 43210, USA
[3]Sandia National Laboratories, Albuquerque, New Mexico 87185, USA

[a)]Author to whom correspondence should be addressed: dominicmerwinxavier.1@buckeyemail.osu.edu

ABSTRACT

Ultra-violet (UV) light emitting diodes operating at 339 nm using transparent interband tunnel junctions are reported. Tunneling-based ultraviolet light emitting diodes were grown by plasma-assisted molecular beam epitaxy on 30% Al-content AlGaN layers. A low tunnel junction voltage drop is obtained through the use of compositionally graded n and p-type layers in the tunnel junction, which enhance hole density and tunneling rates. The transparent tunnel junction-based UV LED reported here show a low voltage drop of 5.55 V at 20 A/cm^2 and an on-wafer external quantum efficiency of 1.02% at 80 A/cm^2.

In recent years, III-nitride ultraviolet (UV) light emitting diodes (LEDs) and lasers have attracted great research interest due to a wide range of applications in air/water purification, disinfection, sterilization, and sensing.[1–3] LEDs and lasers are advantageous over conventional gas-based lamps due to compact size, low power consumption, and safety.[4] Considerable efforts have been made in increasing the radiative efficiency by improving substrate and active region quality.[5–8] However, conventional UV LEDs still have significantly low external quantum and wall plug efficiency compared to their visible counterparts.

One of the major challenges in conventional LEDs is the difficulty to make ohmic contact to the p-AlGaN layer due to its doping limitations. Hence, a p-GaN[9–13] layer or an AlGaN/AlGaN(GaN)[14,15] superlattice is adopted to make ohmic contact which leads to absorption and electrical losses, respectively. In addition to this, the acceptor activation energy in AlGaN is high and increases with the increase in the Al content in AlGaN.[16] This results in low hole concentration in p-layers. An efficient solution to overcome the above-mentioned challenges associated with the poor conductivity and p-type doping in AlGaN in a conventional LED is the use of tunnel junctions (TJs).[17,18] Although GaN based transparent tunnel junctions with low resistances have extensively been studied,[19–22] reports on AlGaN based transparent TJs are relatively few. Previous work on AlGaN TJs with InGaN[23–28] and GaN[29,30,33] as interlayers have shown very low voltage drop, but these interlayers have their own disadvantages as they absorb UV light. In addition, InGaN can only be grown at lower temperatures leading to growth interruptions which may lead to deterioration in the crystal quality.[31] These result in a lower external quantum efficiency (EQE). On the other hand, previously reported transparent homojunction tunnel junctions (HJ TJs)[32–34,38] showed significantly higher voltage losses leading to a lower wall plug efficiency. The higher tunnel junction resistance is because of the increase in tunneling barrier height with the increase in the material bandgap. The poor tunneling probability is also due to the lower hole concentration due to higher activation energy with the increase in the AlGaN composition. Therefore, in addition to degenerate doping, polarization induced charges could also be used in the tunnel junction region by compositional grading. In this work, we show that a combination of compositional grading and high doping can enable a fully transparent $Al_{0.3}Ga_{0.7}N$ (Al-content $\geq$ 30%) transparent tunnel junction with a voltage drop as low as 1.86 V across the tunnel junction at 20 A/cm^2.

To analyze the effects of grading, two PN + TJ (NPN) diodes (displayed in Fig. 1) were first grown on metal–organic chemical vapor deposition (MOCVD)-grown n-type $Al_{0.3}Ga_{0.7}N$ templates (5×10^{18} cm^{-3} Si doping) with a threading dislocation density (TDD) of 2×10^9 cm^{-2}. The samples were grown using Veeco Gen 930 N_2 plasma assisted molecular beam epitaxy (PAMBE) using standard effusion cells for Ga, Mg, Al, and Si at a plasma power of 300 W and a N_2 flow rate of 2.25 sccm corresponding to a growth rate of 246 nm/h. The PN part of the device consists

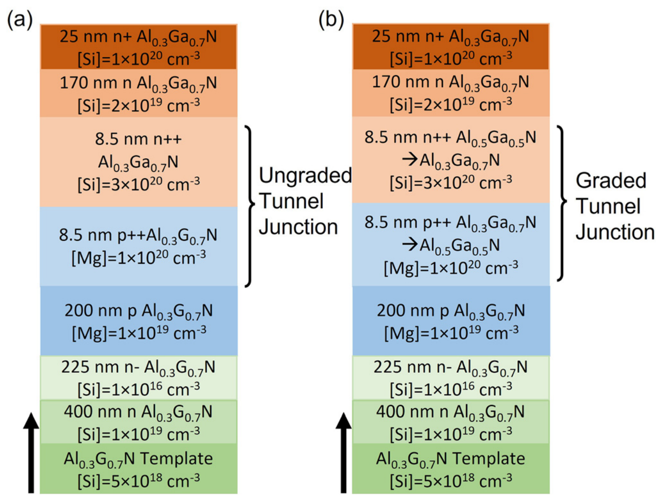

FIG. 1. The epitaxial structure of NPN diodes with (a) ungraded and (b) graded TJs.

of the following epilayers: a 400 nm n $Al_{0.3}Ga_{0.7}N$ buffer layer ($1 \times 10^{19}\,cm^{-3}$ Si doping), a 225 nm n-$Al_{0.3}Ga_{0.7}N$ ($1 \times 10^{17}\,cm^{-3}$ Si doping), and a 200 nm p $Al_{0.3}Ga_{0.7}N$ ($1 \times 10^{19}\,cm^{-3}$ Mg doping). The TJ epistack varies for the two samples. The graded tunnel junction has $p^{++} - Al_{0.5}Ga_{0.5}N \rightarrow p^{++} - Al_{0.3}Ga_{0.7}N$ ($Mg = 1 \times 10^{20}\,cm^{-3}$) and $n^{++} - Al_{0.3}Ga_{0.7}N \rightarrow n^{++} - Al_{0.5}Ga_{0.5}N$ ($Si = 3 \times 10^{20}\,cm^{-3}$) to take advantage of induced 3D polarization charges. The ungraded TJ has $p^{++} - Al_{0.3}Ga_{0.7}N$ ($Mg = 1 \times 10^{20}\,cm^{-3}$) and $n^{++} - Al_{0.3}Ga_{0.7}N$ ($Si = 3 \times 10^{20}\,cm^{-3}$). Both the growths were terminated by a 170 nm n $Al_{0.3}Ga_{0.7}N$ and a 25 nm $n^{+} - Al_{0.3}Ga_{0.7}N$ ($Si = 1 \times 10^{20}\,cm^{-3}$).

The device structures were then fabricated starting with defining square mesas by inductively coupled plasma and reactive ion etching (ICP-RIE) using $BCl_3/Cl_2/Ar$ etch chemistry. This was followed by metal deposition for the top and bottom contacts. The bottom metal stack consists of Ti (20 nm)/Al (120 nm)/Ni (30 nm)/Au (50 nm) annealed in N_2 atmosphere at 850 °C, and the non-alloyed top contact consists of Al (30 nm)/Ni (30 nm)/Au (50 nm). Current density–voltage (J–V) characteristics were measured using a Keysight B1500A semiconductor device analyzer.

Transfer length measurements were performed to extract the contact resistances of the top and bottom layers. The bottom contact resistance was $9 \times 10^{-6}\,\Omega\,cm^2$ for both the device structures and the top contact resistances were 1.61×10^{-4} and $2.2 \times 10^{-6}\,\Omega\,cm^2$ for the ungraded and graded tunnel junction structures, respectively. The difference in the contact resistances can be due to the variations in growth. The total voltage drop at 20 A/cm^2 for is 5.26 and 5.77 for the graded and ungraded TJs, respectively (Fig. 2a). The differential resistance for the two devices was calculated by subtracting the contact resistances and neglecting the diode resistance. This sets an upper threshold limit of $8.9 \times 10^{-5}\,\Omega\,cm^2$ for the graded TJ structure and $6.9 \times 10^{-3}\,\Omega\,cm^2$ for the ungraded TJ structure (Fig. 2b). The graded TJ structure has the lowest reported differential resistance for any AlGaN based TJ (Fig. 2e).[23,25,26,37,38] Simulations of the TJ structures were carried out using Silvaco Atlas TCAD. The non-local band to band tunneling model was used to calculate the tunneling rates in both the heavily doped n and p regions. When the n and p layers are

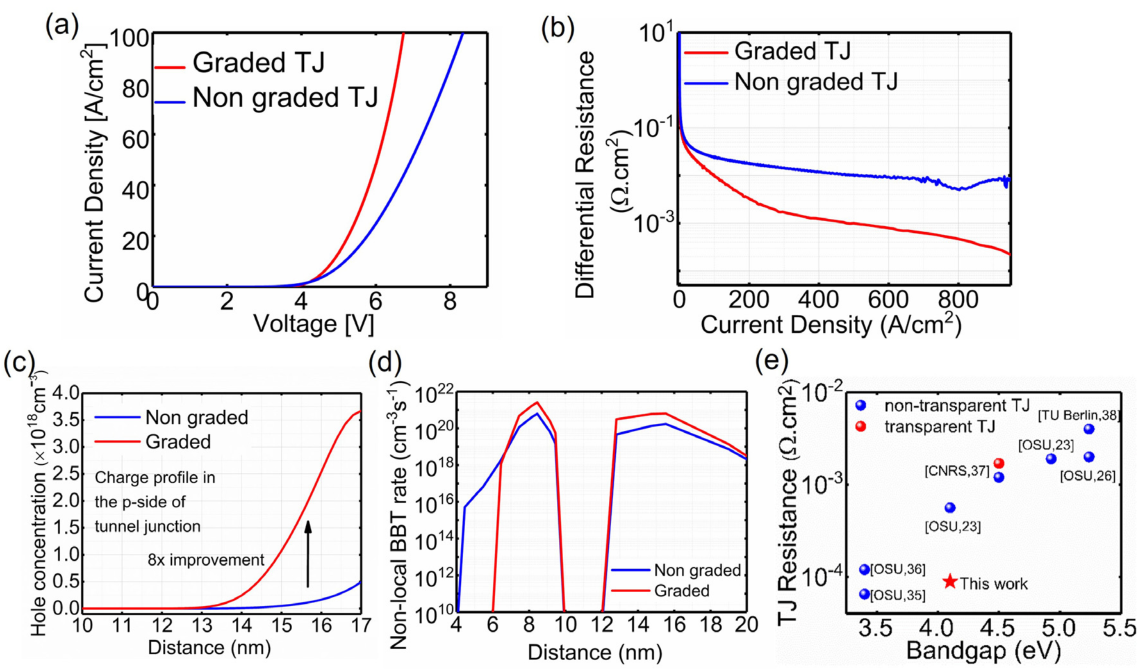

FIG. 2. (a) Experimental current density profile, (b) differential resistance as a function of current density, (c) simulated hole concentration profiles on the p++ layers of the tunnel junction, (d) simulated band to band tunneling rate of not-graded and graded tunnel junctions, and (e) reported TJ resistance as a function of bandgap for different UV LEDs.[23,25,26,33,35–38]

compositionally graded, the polarization charges induce large concentrations of free carriers in the tunnel junction region,[39–41] reducing depletion related tunneling barriers. It also improves the tunneling probability at reduced bias. The modeling predicts that linearly grading from 50% Al to 30% Al on the p side increases the hole concentration eightfold, and tunneling rate fourfold compared with a non-graded junction (Fig. 2c,d).

Following the NPN diode structures, the graded TJ was then grown on top of LED devices The epitaxial structure of the tunnel junction-based UV LED is shown in Fig. 3(a) and the corresponding equilibrium energy band diagram is shown in Fig. 1(b). The growth was initiated with a 100 nm thick n-$Al_{0.3}Ga_{0.7}N$ buffer layer (1×10^{19} cm^{-3} Si doping). The active region consists of three pairs of 2.5 nm $Al_{0.15}Ga_{0.85}N$ quantum wells and 7 nm $Al_{0.3}Ga_{0.7}N$ quantum barriers, which is followed by a 4 nm $Al_{0.7}Ga_{0.3}$ N electron blocking layer (EBL). The transparent TJ was grown at 700 °C immediately on top of the active region. The grading gives rise to a high concentration of holes very close to the active region. The growth was completed with a 170 nm n-type $Al_{0.3}Ga_{0.7}N$ (2×10^{19} cm^{-3} Si doping) layer and a 25 nm n^+-type $Al_{0.3}Ga_{0.7}N$ (1×10^{20} cm^{-3} Si doping) acting as a contact layer.

The surface morphology of the as-grown epitaxial structure was analyzed using Bruker Icon Dimension atomic force microscopy (AFM). An rms roughness of 1.33 nm was extracted for a scan area of 5×5 μm^2. The absence of step-flow features is attributed to the high Si doping, since Si can act as an anti-surfactant.[42] The $2\theta - \omega$ scan of the LED was measured using a Bruker D8 Discover x-ray diffraction (XRD) system. Simulated thickness/composition values [Fig. 3(a)] and experimental peaks/fringes were found to match fairly well, as shown in Fig. 3(d).

The LED device structures were fabricated using the same process as that of the PN + TJ didoes. Apart from J–V measurements, capacitance–voltage (C–V) measurements were carried out by reverse biasing the top *n*-contact with an excitation frequency of 5 MHz and an amplitude of 30 mV. Electroluminescence (EL) peaks were obtained from on-wafer measurement at room temperature using a calibrated Ocean Optics USB 2000 spectrometer coupled with a fiber optic cable. The external quantum efficiency (EQE) of the device was measured from the output power collected using a Thorlabs PM100D optical power meter fitted with a S120VC photodiode power sensor.

The TJ and the LEDs were separately simulated using doping density values similar to the MBE grown LED. The polarization charges in the graded layers of the tunnel junction and at the quantum well/barrier interface in the LED was based on previously calculated values.[43] Since the tunnel junction is at a significant distance from the active region, we expect that simulating these two components separately and adding the voltage can predict the voltage drop of the full TJ-LED structure.

The on-wafer room-temperature electrical characteristics are shown in Fig. 4. Measured electrical characteristics of the fabricated LED (100×100 μm^2) are shown in Fig. 4(a), together with the simulated characteristics for the LED. In the case of the simulation, the voltage drop for TJ, LED, and the sum of the simulated TJ and LED voltage drops are shown. At 20 A/cm^2, the experimental device exhibits a forward voltage of 5.55 V. This compares well with the simulated voltage drop (~5.7 V), which is the combination of the tunnel junction loss (1.4 V) and the voltage drop across the active region (4.3 V) at 20 A/cm^2. Top-down CV measurements were done on 40 μm diameter circular pads, and a zero-bias depletion width of 41 nm [Fig. 4(b)] was extracted, approximately matching the expected depletion width from the equilibrium energy band diagram [Fig. 3(b)]. The C–V profile is relatively flat with respect to bias due to the heavy doping in the p- and n-regions. The effective charge density with respect to the depletion width is shown in Fig. 4(c). The peak near zero bias depletion width may be attributed to electron accumulation in the bottom-most quantum well. At larger reverse bias, depletion width expands, and the C–V profile suggests an apparent carrier density

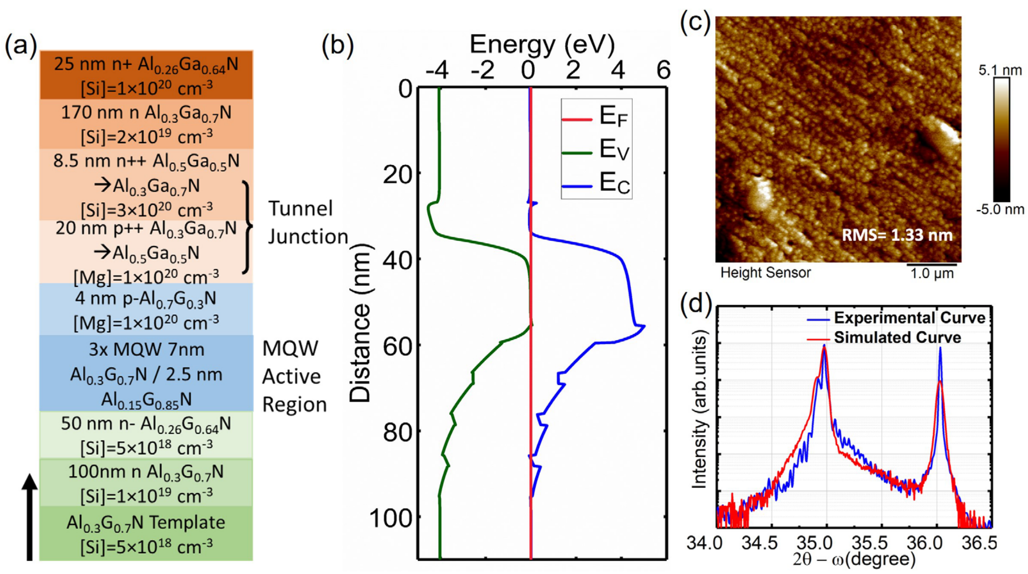

FIG. 3. (a) The epitaxial structure and (b) energy band diagram of the designed UV-LED. (c) 5 $\mu m \times 5$ μm AFM scan. (d) Experimental and simulated HR-XRD profiles of the MBE grown LED.

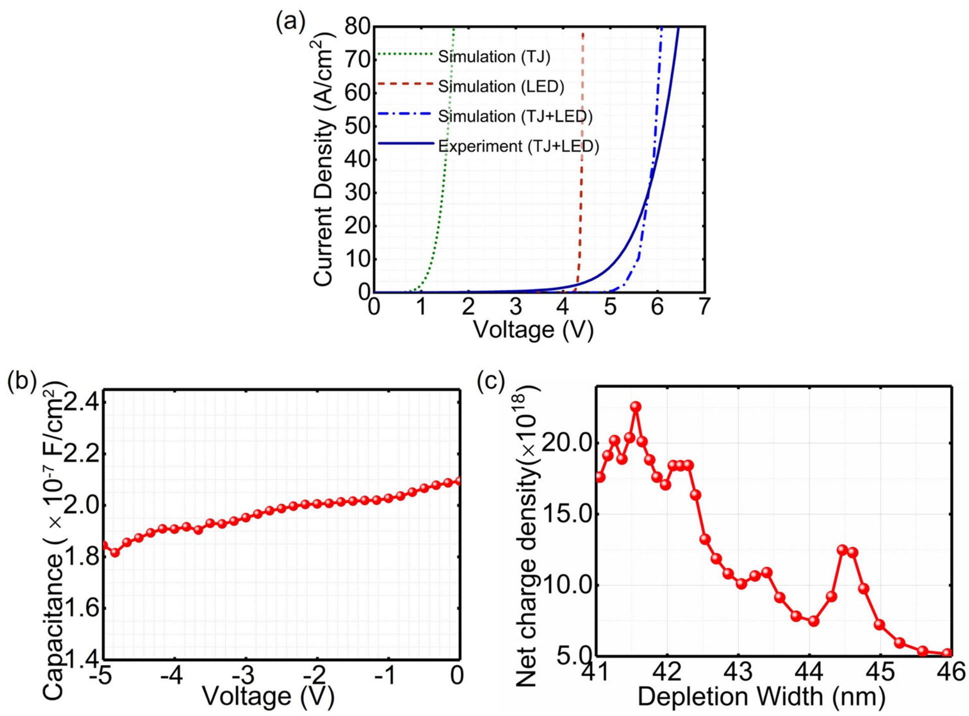

FIG. 4. (a) Simulated and experimental J–V characteristics. (b) Measured C–V characteristics. (c) Extracted net charge densities of the MBE grown TJ-UV LED.

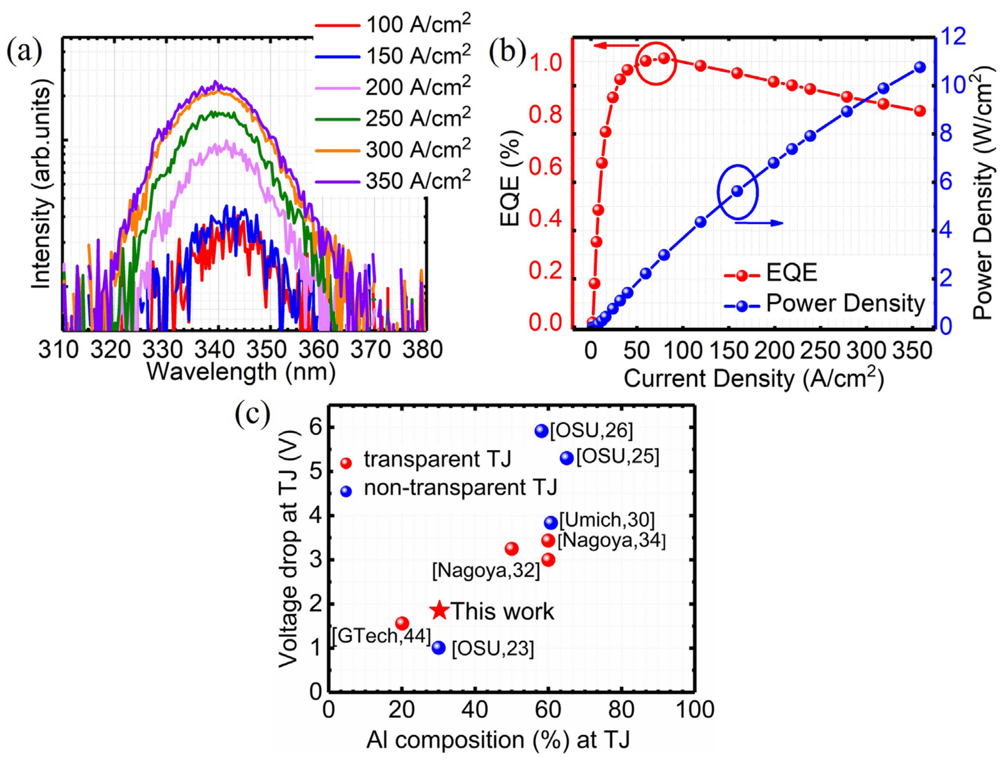

FIG. 5. (a) Electroluminescence spectra, (b) output power density and the external quantum efficiency LED under CW operations. (c) Voltage drop across the tunnel junction as a function of Al composition (%) at the tunnel junction for various TJ-UV LEDs.[23,25,26,30,32,34,44]

$\sim 5 \times 10^{18}\,cm^{-3}$, which is similar to the predicted doping density. Capacitance at higher reverse bias could not be measured due to leakage and increase in the loss tangent of the test structures. Transfer length measurement patterns were characterized on the top and bottom layers. The ohmic behavior was observed for both contacts, with a sheet resistance of 786 and 92Ω/□ and a contact resistance of 1.24×10^{-4} and $1.29 \times 10^{-5}\,\Omega\,cm^2$ for the bottom and top contact layers, respectively.

Electroluminescence measurements carried out on a $100 \times 100\,\mu m^2$LED at different current levels ranging from 100 to 350 A/cm^2 indicate a single peak at 339 nm at 350 A/cm^2 which blue-shifted from 343 nm at 100 A/cm^2 due to both quantum stark confined effect and band filling effect [shown in Fig. 5(a)]. No secondary peaks were observed in the measurement. On-wafer measurements show a peak EQE of 1.02% at a current density of 80 A/cm^2. The emission power spectrum with respect to the current density is shown in Fig. 5(b)—the values reported here correspond to direct measurements from the calibrated detector with no corrections for light extraction were made. An optical output power density of 10.7 W/cm^2 is recorded for a current density of 358 A/cm^2. Since these measurements were made on-wafer without an integrating sphere, the EQE and power density values may be underestimated. Figure 5(c) shows the voltage drop across the tunnel junction at 20 A/cm^2 for previously reported tunnel junction-based UV LEDs as a function of the Al composition (%) across the tunnel junction layers. The tunnel junction voltage drop was estimated as the difference between the total voltage drop of the LED measured at 20 A/cm^2 and the bandgap of the quantum wells (assumed to be the same as the emission spectrum peak photon energy) except for Ref. 32. In Ref. 32, the tunnel junction drop is calculated by taking the total voltage drop at 20 A/cm^2 and subtracting the voltage drop at 20 A/cm^2 from the PN junction mentioned in Ref. 32. Previously reported transparent tunnel junctions (red spheres) showed relatively high operating voltages, while the use of InGaN and GaN interlayers within TJs has typically led to better performance. Our results show that a combination of high doping and compositional grading can enable low forward voltage drop, at least at Al-content in the range discussed here.

In summary, we have demonstrated low voltage drop transparent tunnel junctions with Al content $\geq$ 30% in the tunnel junction grown by molecular beam epitaxy for UV-B LEDs. With a 30% Al composition, emission wavelengths in the UVA and UVB region (up to 300 nm wavelength) can be obtained for various applications. The device exhibited a peak EQE of 1.02% and an output power density of 10.76 W/cm^2, which indicates excellent hole injection through the tunnel junction. The efficiency of these LEDs could be further improved by optimizing the active region design. Such low voltage drop transparent tunnel junction at high Al-content will be beneficial for higher current density applications like lasers and cascading LEDs.

This research was funded by the National Science Foundation (NSF) under Grant No. 2034140.

AUTHOR DECLARATIONS

Conflict of Interest

The authors have no conflicts to disclose.

Author Contributions

Agnes Maneesha Dominic Merwin Xavier: Conceptualization (equal); Data curation (lead); Formal analysis (lead); Investigation (equal); Visualization (equal); Writing – original draft (lead); Writing – review & editing (equal). **Arnob Ghosh:** Data curation (equal); Formal analysis (supporting); Writing – review & editing (equal). **Sheikh Ifatur Rahman:** Data curation (supporting); Formal analysis (supporting); Visualization (equal); Writing – original draft (equal); Writing – review & editing (equal). **Andrew A. Allerman:** Investigation (supporting); Resources (equal); Writing – review & editing (supporting). **Shamsul Arafin:** Funding acquisition (equal); Investigation (equal); Project administration (equal); Resources (equal); Supervision (equal); Validation (equal); Writing – review & editing (supporting). **Siddharth Rajan:** Conceptualization (equal); Funding acquisition (equal); Investigation (equal); Project administration (equal); Resources (equal); Supervision (equal); Validation (equal); Writing – review & editing (equal).

DATA AVAILABILITY

The data that support the findings of this study are available from the corresponding author upon reasonable request.

REFERENCES

[1]S. L. Miller, J. Linnes, and J. Luongo, "Ultraviolet germicidal irradiation: Future directions for air disinfection and building applications," Photochem. Photobiol. **89**(4), 777–781 (2013).
[2]K. Song, M. Mohseni, and F. Taghipour, "Application of ultraviolet light-emitting diodes (UV-LEDs) for water disinfection: A review," Water Res. **94**, 341–349 (2016).
[3]M. Mori, A. Hamamoto, A. Takahashi, M. Nakano, N. Wakikawa, S. Tachibana, T. Ikehara, Y. Nakaya, M. Akutagawa, and Y. Kinouchi, "Development of a new water sterilization device with a 365 nm UV-LED," Medi. Biol. Eng. Comput. **45**(12), 1237–1241 (2007).
[4]Y. Muramoto, M. Kimura, and S. Nouda, "Development and future of ultraviolet light-emitting diodes: UV-LED will replace the UV lamp," Semicond. Sci. Technol. **29**(8), 084004 (2014).
[5]H. Hirayama, N. Maeda, S. Fujikawa, S. Toyoda, and N. Kamata, "Recent progress and future prospects of AlGaN-based high-efficiency deep-ultraviolet light-emitting diodes," Jpn. J. Appl. Phys., Part 1 **53**(10), 100209 (2014).
[6]Z. Bryan, I. Bryan, J. Xie, S. Mita, Z. Sitar, and R. Collazo, "High internal quantum efficiency in AlGaN multiple quantum wells grown on bulk AlN substrates," Appl. Phys. Lett. **106**(14), 142107 (2015).
[7]S. Sen, C. Singha, A. Saha, A. Das, P. Guha Roy, P. Pramanik, and A. Bhattacharyya, "AlGaN multiple quantum wells by PA-MBE for deep UV emission: Effect of growth interruptions," J. Cryst. Growth **523**, 125159 (2019).
[8]A. Bhattacharyya, T. D. Moustakas, L. Zhou, D. J. Smith, and W. Hug, "Deep ultraviolet emitting AlGaN quantum wells with high internal quantum efficiency," Appl. Phys. Lett. **94**(18), 181907 (2009).
[9]Y. Liao, C. Thomidis, C.-K. Kao, and T. D. Moustakas, "AlGaN based deep ultraviolet light emitting diodes with high internal quantum efficiency grown by molecular beam epitaxy," Appl. Phys. Lett. **98**(8), 081110 (2011).
[10]T. Wang, Y. Liu, Y. Lee, Y. Izumi, J. Ao, J. Bai, H. Li, and S. Sakai, "Fabrication of high performance of AlGaN/GaN-based UV light-emitting diodes," J. Cryst. Growth **235**(1–4), 177–182 (2002).
[11]G. Yang, F. Xie, K. Dong, P. Chen, J. Xue, T. Zhi, T. Tao, B. Liu, Z. Xie, and X. Xiu, "Design of deep ultraviolet light-emitting diodes with staggered AlGaN quantum wells," Physica E **62**, 55–58 (2014).
[12]J. Yan, J. Wang, P. Cong, L. Sun, N. Liu, Z. Liu, C. Zhao, and J. Li, "Improved performance of UV-LED by p-AlGaN with graded composition," Phys. Status Solidi C **8**(2), 461–463 (2011).
[13]B. K. SaifAddin, A. S. Almogbel, C. J. Zollner, F. Wu, B. Bonef, M. Iza, S. Nakamura, S. P. DenBaars, and J. S. Speck, "AlGaN deep-ultraviolet light-emitting diodes grown on SiC substrates," ACS Photonics **7**(3), 554–561 (2020).
[14]J.-Y. Duboz, "GaN/AlGaN superlattices for p contacts in LEDs," Semicond. Sci. Technol. **29**(3), 035017 (2014).

[15]T.-Y. Wang, W.-C. Lai, S.-Y. Sie, S.-P. Chang, C.-H. Kuo, and J.-K. Sheu, "Deep ultraviolet AlGaN-based light-emitting diodes with p-AlGaN/AlGaN superlattice hole injection structures," Processes **9**(10), 1727 (2021).
[16]M. S. Hasan, I. M. Mehedi, S. M. F. Reza, M. R. Kaysir, and M. R. Islam, "Analytical investigation of activation energy for Mg-doped p-AlGaN," Opt. Quantum Electron. **52**(7), 348 (2020).
[17]S. Krishnamoorthy, D. N. Nath, F. Akyol, P. S. Park, M. Esposto, and S. Rajan, "Polarization-engineered GaN/InGaN/GaN tunnel diodes," Appl. Phys. Lett. **97**(20), 203502 (2010).
[18]M. J. Grundmann and U. K. Mishra, "Multi-color light emitting diode using polarization-induced tunnel junctions," Phys. Status Solidi C **4**(7), 2830–2833 (2007).
[19]Z. Jamal-Eddine, S. M. N. Hasan, B. Gunning, H. Chandrasekar, M. Crawford, A. Armstrong, S. Arafin, and S. Rajan, "Low voltage drop tunnel junctions grown monolithically by MOCVD," Appl. Phys. Lett. **118**(5), 053503 (2021).
[20]Y. Akatsuka, S. Iwayama, T. Takeuchi, S. Kamiyama, M. Iwaya, and I. Akasaki, "Doping profiles in low resistive GaN tunnel junctions grown by metalorganic vapor phase epitaxy," Appl. Phys. Express **12**(2), 025502 (2019).
[21]S. M. N. Hasan, B. P. Gunning, Z. J. Eddine, H. Chandrasekar, M. H. Crawford, A. Armstrong, S. Rajan, and S. Arafin, "All-MOCVD-grown gallium nitride diodes with ultra-low resistance tunnel junctions," J. Phys. D **54**(15), 155103 (2021).
[22]J. Wang, E. C. Young, W. Y. Ho, B. Bonef, T. Margalith, and J. S. Speck, "III-nitride blue light-emitting diodes utilizing hybrid tunnel junction with low excess voltage," Semicond. Sci. Technol. **35**(12), 125026 (2020).
[23]Y. Zhang, S. Krishnamoorthy, J. M. Johnson, F. Akyol, A. Allerman, M. W. Moseley, A. Armstrong, J. Hwang, and S. Rajan, "Interband tunneling for hole injection in III-nitride ultraviolet emitters," Appl. Phys. Lett. **106**(14), 141103 (2015).
[24]Y. Zhang, S. Krishnamoorthy, F. Akyol, A. A. Allerman, M. W. Moseley, A. M. Armstrong, and S. Rajan, "Design and demonstration of ultra-wide bandgap AlGaN tunnel junctions," Appl. Phys. Lett. **109**(12), 121102 (2016).
[25]Y. Zhang, S. Krishnamoorthy, F. Akyol, S. Bajaj, A. A. Allerman, M. W. Moseley, A. M. Armstrong, and S. Rajan, "Tunnel-injected sub-260 nm ultraviolet light emitting diodes," Appl. Phys. Lett. **110**(20), 201102 (2017).
[26]Y. Zhang, Z. Jamal-Eddine, F. Akyol, S. Bajaj, J. M. Johnson, G. Calderon, A. A. Allerman, M. W. Moseley, A. M. Armstrong, and J. Hwang, "Tunnel-injected sub 290 nm ultra-violet light emitting diodes with 2.8% external quantum efficiency," Appl. Phys. Lett. **112**(7), 071107 (2018).
[27]Y. Zhang, S. Krishnamoorthy, F. Akyol, J. M. Johnson, A. A. Allerman, M. W. Moseley, A. M. Armstrong, J. Hwang, and S. Rajan, "Reflective metal/semiconductor tunnel junctions for hole injection in AlGaN UV LEDs," Appl. Phys. Lett. **111**(5), 051104 (2017).
[28]Y. Zhang, S. Krishnamoorthy, F. Akyol, A. A. Allerman, M. W. Moseley, A. M. Armstrong, and S. Rajan, "Design of p-type cladding layers for tunnel-injected UV-A light emitting diodes," Appl. Phys. Lett. **109**(19), 191105 (2016).
[29]A. Pandey, J. Gim, R. Hovden, and Z. Mi, "An AlGaN tunnel junction light emitting diode operating at 255 nm," Appl. Phys. Lett. **117**(24), 241101 (2020).
[30]A. Pandey, W. J. Shin, J. Gim, R. Hovden, and Z. Mi, "High-efficiency AlGaN/GaN/AlGaN tunnel junction ultraviolet light-emitting diodes," Photonics Res. **8**(3), 331–337 (2020).
[31]I. Mayboroda, A. Knizhnik, Y. V. Grishchenko, I. Ezubchenko, M. L. Zanaveskin, O. Kondratev, M. Y. Presniakov, B. Potapkin, and V. Ilyin, "Growth of AlGaN under the conditions of significant gallium evaporation: Phase separation and enhanced lateral growth," J. Appl. Phys. **122**(10), 105305 (2017).
[32]K. Nagata, H. Makino, H. Miwa, S. Matsui, S. Boyama, Y. Saito, M. Kushimoto, Y. Honda, T. Takeuchi, and H. Amano, "Reduction in operating voltage of AlGaN homojunction tunnel junction deep-UV light-emitting diodes by controlling impurity concentrations," Appl. Phys. Express **14**(8), 084001 (2021).
[33]F. Mehnke, C. Kuhn, M. Guttmann, L. Sulmoni, V. Montag, J. Glaab, T. Wernicke, and M. Kneissl, "Electrical and optical characteristics of highly transparent MOVPE-grown AlGaN-based tunnel heterojunction LEDs emitting at 232 nm," Photonics Research **9**(6), 1117–1123 (2021).
[34]K. Nagata, S. Anada, H. Miwa, S. Matsui, S. Boyama, Y. Saito, M. Kushimoto, Y. Honda, T. Takeuchi, and H. Amano, "Structural design optimization of 279 nm wavelength AlGaN homojunction tunnel junction deep-UV light-emitting diode," Appl. Phys. Express **15**(4), 044003 (2022).
[35]F. Akyol, Y. Zhang, S. Krishnamoorthy, and S. Rajan, "Ultralow-voltage-drop GaN/InGaN/GaN tunnel junctions with 12% indium content," Appl. Phys. Express **10**(12), 121003 (2017).
[36]S. Krishnamoorthy, F. Akyol, P. S. Park, and S. Rajan, "Low resistance GaN/InGaN/GaN tunnel junctions," Appl. Phys. Lett. **102**(11), 113503 (2013).
[37]V. F. Arcara, B. Damilano, G. Feuillet, S. Vézian, K. Ayadi, S. Chenot, and J.-Y. Duboz, "Ge doped GaN and $Al_{0.5}Ga_{0.5}N$-based tunnel junctions on top of visible and UV light emitting diodes," J. Appl. Phys. **126**(22), 224503 (2019).
[38]C. Kuhn, L. Sulmoni, M. Guttmann, J. Glaab, N. Susilo, T. Wernicke, M. Weyers, and M. Kneissl, "MOVPE-grown AlGaN-based tunnel heterojunctions enabling fully transparent UVC LEDs," Photonics Res. **7**(5), B7–B11 (2019).
[39]J. Simon, V. Protasenko, C. Lian, H. Xing, and D. Jena, "Polarization-induced hole doping in wide-band-gap uniaxial semiconductor heterostructures," Science **327**(5961), 60–64 (2010).
[40]P. Sung Park, D. N. Nath, S. Krishnamoorthy, and S. Rajan, "Electron gas dimensionality engineering in AlGaN/GaN high electron mobility transistors using polarization," Appl. Phys. Lett. **100**(6), 063507 (2012).
[41]R. Dalmau and B. Moody, "Polarization-induced doping in graded AlGaN epilayers grown on AlN single crystal substrates," ECS Trans. **86**(12), 31 (2018).
[42]Z. Benzarti, I. Halidou, O. Tottereau, T. Boufaden, and B. E. Jani, "Silicon effect on GaN surface morphology," Microelectron. J. **33**(11), 995–998 (2002).
[43]F. Bernardini, V. Fiorentini, and D. Vanderbilt, "Spontaneous polarization and piezoelectric constants of III-V nitrides," Phys. Rev. B **56**(16), R10024 (1997).
[44]E. A. Clinton, Z. Engel, E. Vadiee, J. V. Carpenter, Z. C. Holman, and W. A. Doolittle, "Ultra-wide-bandgap AlGaN homojunction tunnel diodes with negative differential resistance," Appl. Phys. Lett. **115**(8), 082104 (2019).